Highly Efficient and Selective Recovery of Rare Earth Elements Using Mesoporous Silica Functionalized by Preorganized Chelating Ligands

*Yimu Hu,[a,b,c] Elisabeth Drouin,[a,c] Dominic Larivière,[*a,c] Freddy Kleitz,[*a,b,d] and Frédéric-Georges Fontaine[*a,c]*

[a] Department of Chemistry, Université Laval, Québec, G1V 0A6, QC, Canada

[b] Centre de Recherche sur les Matériaux Avancés (CERMA), Université Laval, Québec, G1V 0A6, QC, Canada

[c] Centre en Catalyse et Chimie Verte (C3V), Université Laval, Québec, G1V 0A6, QC, Canada

[d] Department of Inorganic Chemistry – Functional Materials, Faculty of Chemistry, University of Vienna, 1090 Vienna, Austria

E-mails: frederic.fontaine@chm.ulaval.ca and dominic.larriviere@chm.ulaval.ca.and freddy.kleitz@univie.ac.at

This is the peer reviewed version of the following article: [Highly Efficient and Selective Recovery of Rare Earth Elements Using Mesoporous Silica Functionalized by Preorganized Chelating Ligands, ACS Appl. Mater. Interfaces 2017, 9, 38584−38593], which has been published in final form at [10.1021/acsami.7b12589].

Highly Efficient and Selective Recovery of Rare Earth Elements Using Mesoporous Silica Functionalized by Preorganized Chelating Ligands

Yimu Hu,[a,b,c] Elisabeth Drouin,[a,c] Dominic Larivière,[*a,c] Freddy Kleitz,[*a,b,d] and Frédéric-Georges Fontaine[*a,c]

[a] Department of Chemistry, Université Laval, Québec, G1V 0A6, QC, Canada

[b] Centre de Recherche sur les Matériaux Avancés (CERMA), Université Laval, Québec, G1V 0A6, QC, Canada

[c] Centre en Catalyse et Chimie Verte (C3V), Université Laval, Québec, G1V 0A6, QC, Canada

[d] Department of Inorganic Chemistry – Functional Materials, Faculty of Chemistry, University of Vienna, 1090 Vienna,

Austria

ABSTRACT: Separating the rare earth elements (REEs) in an economically and environmentally sustainable manner is one of the most pressing technological issues of our time. Herein, a series of preorganized bidentate phthaloyl diamide (PA) ligands were synthesized and grafted on large-pore 3-dimensional (3-D) KIT-6 mesoporous silica. The synthesized sorbents were fully characterized by N_2 physisorption, FT-IR, ^{13}C cross polarization (CP) and ^{29}Si magic-angle spinning (MAS) NMR, thermogravimetric analysis-differential thermal analysis (TGA-DTA), and elemental analysis. Overall, the grafting of PA-type ligands was found to have significantly improved the extraction performance of the sorbents towards REEs compared to the homogeneous analogues. Specifically, the sorbent modified with the 1,2-phtaloyl ligand shows high preference over lanthanides with smaller size, whereas the 1,3-phtaloyl ligand exhibit selectivity towards elements with larger ion radius. This selectivity drastically changes from the homogeneous models that do not exhibit any selectivity. The possibility of regenerating mesoporous sorbents through simple stripping using oxalate salt is demonstrated over up to 10 cycles with no significant loss in REEs extraction capacity, suggesting adequate chemical and structural stability of the new sorbent materials. Despite of the complex ion matrix and high ionic composition, the exposure of industrial mining deposits containing REEs to the sorbents results in selective recovery of target REEs.

KEYWORDS: mesoporous silica, rare earth elements, lanthanides, selective extraction, KIT-6

1. INTRODUCTION

The rare-earth elements (REEs), consisting of primarily the 15 lanthanides (Ln) as well as scandium (Sc) and yttrium (Y), are essential elements for modern technologies. The importance of REEs has been booming owing to their unique electronic, magnetic, and optical properties, and their wide applications in electronics, metallurgy, and catalysis.[1,2] The emerging concept of clean and low-carbon energy technology, such as electric vehicles, wind power, and energy-efficient lighting, has further boosted the demand for such technological materials. Nowadays, the rare earth industry is dominated by China, who contributes to more than 90% of the global production;[3] however, since 2010 China has restricted the exportation of REE resources notably due to increasing concerns for environmental effects of mining. Because of their necessity in the clean energy economy and the vulnerability of supply shortage, REEs have been classified as critical materials by the U.S. Department of Energy[4] and the European Union.[5]

Contrary to their name, rare earth elements are moderately abundant in the earth's crust; however, they are often unfavorably distributed in common ores/minerals, and are rarely present in economically exploitable concentrations.[6,7] Moreover, the similarity in physicochemical properties between adjacent REEs renders the separation of individual elements extremely difficult. Indeed, the bottleneck in securing the REE supply chain lies in the lack of efficient separation methodologies. The most commonly used technologies in the industry are multiple step liquid-liquid extraction (LLE) and resin-based chromatography (supported-liquid extraction, SLE). The LLE process has limited selectivity and consumes large

amount of organic solvent during repetitive extraction cycles and generates undesired waste, whereas the SLE suffers from the lack of reusability and high cost. In comparison, the emerging solid-phase extraction (SPE) systems require less solvent and provide better separation factors, and thus are promising sample treatment techniques.[8] In this regard, porous silica materials have received great attention because of their superior extraction capacity and stability.[9] In particular, ordered mesoporous silica materials (OMSs) possess large surface area, well-defined pore size, chemical stability, and are easily modified by organic ligands, thus yielding functionalized materials with enhanced separation and analytical performance. For example, after grafting of diglycolyamide (DGA) on mesoporous KIT-6 silica,[10] and maleic acid on MCM-41,[11] the resulting hybrid materials exhibited high sorption capacity and enhanced selectivity towards REEs. In addition, ordered SBA-15-type Dy^{3+} ion-imprinted mesoporous silica modified by acetylacetone was designed for specific recovery of Dy^{3+} in acidic media.[12] It has been suggested that compared to two-dimensional (2-D) hexagonal mesoporous supports, such as SBA-15 and MCM-41, the large-pore, interconnected and three-dimensional (3-D) cubic nature of a KIT-6 support reduces the risk of pore blocking during functionalization with large molecules, and facilitates the mass transport of the solution during adsorption.[13–16]

From a chemical point of view, the discovery of ligands with superior selectivity would play a critical role in enhancing the extraction performance of sorbents. The Ln^{3+} cations are highly Lewis acidic and easily coordinate nucleophiles, with a clear preference towards oxygen donors. A fundamental challenge for the design of such ligands lies in differencing various REEs with radii ranging from 74.5 pm for Sc^{3+} to 103.2 pm for La^{3+}. To date, only a few size-based separation agents have been investigated.[17–21] One of our recent studies shows that by tuning the *bite angle* formed by chelating ligands, a certain degree of selectivity towards REEs could be achieved.[19] For example, the derivative of 3,6-dioxaoctanediamide (DOODA) has a smaller *bite angle* than the DGA ligand, and the mesoporous KIT-6 silica functionalized with DOODA shows preference for smaller lanthanides. However, the rotation of the σ-σ bond in DGA and DOODA might have an adverse effect on the rigidity of hybrid materials, thus hampering their selectivity. The concept of "ligand preorganization" has been brought up to attention, and most of the preorganized ligands to date are mixed soft N-donor and hard O-donor extractants for the selective enrichment of actinides.[15,22–24] In this work, we synthesized a series of ligands based on phthaloyl diamide (PA) bearing different *bite angles* by varying the position of carbonyl group on the aromatic ring. The conjugated aromatic structure provides a rigid structure, making phthaloyl diamide preorganized for forming complexes with REEs of different ions radii. The grafting of ligands on the large-pore 3-D cubic KIT-6 silica also decreases the flexibility of the coordinating carbonyl groups, thus further adding to the overall rigidity of the ligand. The hybrid materials exhibit impressive adsorption capacity and selective affinities towards REEs with larger or smaller ion size under batch conditions, when no selectivity is observed with the homogeneous PA analogues. Furthermore, the adsorption mechanism was studied in detail, and dynamic extraction tests were carried out to assess the reusability of the solid-phase sorbents. Finally, the applicability of the sorbents was demonstrated by selective recovery of REEs from two real-world silicate and niobium mining deposits samples.

2. EXPERIMENTAL SECTION

Chemical and materials. Tetraethoxysilane (TEOS, 98%), (3-aminopropyl)triethoxysilane (APTS, 98%), and *N,N*-dioctylamine (97%) were purchased from Sigma-Aldrich. Phthaloyl chloride (94%), isophthaloyl dichloride (98%), and terephthaloyl chloride (99%) were purchased from Alfa Aesar and were used without further purification. Analytical-reagent grade hydrochloric acid (37%), nitric acid (65%), and sodium hydroxide were purchased from Merck and were used without further purification. Toluene (Sigma-Aldrich) and triethylamine (Sigma-Aldrich, 99%) were dried and distilled using Na/benzophenone, and stored on molecular sieves under nitrogen. Solutions of REEs (Y, La, Ce, Pr, Nd, Sm, Eu, Gd, Tb, Dy, Ho, Er, Tm, Yb, Lu) and additional ions (Al and Fe) were prepared from the reference standard solutions (Plasma, Cal, SCP Science) using nanopure water.

Synthesis of 1,2-phthaloyl diamidopropyltriethoxysilane (1,2-PA-APTS). To a solution of phthaloyl chloride (1,2-PACl, 1.53 mL, 10 mmol) in 25 mL of dry toluene, a mixture of APTS (4.9 mL, 21 mmol) and triethylamine (14 mL, 100 mmol) in 20 mL of toluene was slowly added. The reaction was stirred at room temperature overnight. The reaction mixture was then filtrated and the solvent was removed under reduced pressure, yielding a light-yellow solid. Yield: 5.14 g (90%). ^{1}H NMR (DMSO-d_6) δ: 8.22 (br, 2H, NH^{APTS}), 7.45 (m, 4H, aromatics), 3.75 (q, 12H, CH_2–OSi^{APTS}), 3.14 (q, 4H, CH_2–NH^{APTS}), 1.55 (m, 4H, CH_2–CH_2^{APTS}), 1.15 (t, 18H, CH_3^{APTS}), 0.60 (t, 4H, CH_2–Si^{APTS}). ^{13}C{^{1}H} NMR (DMSO-d_6) δ: 168.0 (C=O), 136.4 (1,2-aromatic), 129.1 (3,6-aromatic), 127.6 (4,5-aromatic), 57.7 (CH_2–O–Si^{APTS}), 41.9 (CH_2–NH^{APTS}), 22.6 (CH_2–CH_2^{APTS}), 18.2 (CH_3^{APTS}), 7.4 (CH_2–Si^{APTS}). Elemental Anal. Calc. for $C_{26}H_{48}N_2O_8Si_2$: C, 54.51; H, 8.45; N, 4.89%. Found: C, 54.62; H, 8.42; N, 4.88%.

Synthesis of 1,3-phthaloyl diamidopropyltriethoxysilane (1,3-PA-APTS). To a solution of isophthaloyl dichloride (1,3-PACl, 2.04 g, 10 mmol) in 25 mL of dry toluene at 0 °C, a mixture of APTS (4.9 mL, 21 mmol) and triethylamine (14 mL, 100 mmol) in 20 mL of toluene was slowly added. The reaction was allowed to warm to room temperature and stirred overnight. The reaction mixture was then filtrated and the solvent was removed under reduced pressure, yielding a transparent yellow oil as final product. Yield: 4.94 g (86%). ^{1}H NMR (DMSO-d_6) δ: 8.61 (br, 2H, NH^{APTS}), 8.31 (s, 1H, 3-aromatic), 7.94 (m, 2H, 4,6-aromatics), 7.53 (m, 1H, 5-

aromatics), 3.75 (q, 12H, CH_2–OSi^{APTS}), 3.24 (q, 4H, CH_2–NH^{APTS}), 1.59 (m, 4H, CH_2–CH_2^{APTS}), 1.14 (t, 18H, CH_3^{APTS}), 0.60 (t, 4H, CH_2–Si^{APTS}). $^{13}C\{^1H\}$ NMR (DMSO-d_6) δ: 165.7 (C=O), 134.9 (1,3-aromatic), 129.5 (4,6-aromatic), 128.2 (2-aromatic), 127.2 (5-aromatic), 57.7 (CH_2–O–Si^{APTS}), 42.1 (CH_2–NH^{APTS}), 22.7 (CH_2–CH_2^{APTS}), 18.2 (CH_3^{APTS}), 7.5 (CH_2–Si^{APTS}). Elemental Anal. Calc. for $C_{26}H_{48}N_2O_8Si_2$: C, 54.51; H, 8.45; N, 4.89%. Found: C, 54.71; H, 8.47; N, 4.90%.

Synthesis of 1,4-phthaloyl diamidopropyltriethoxysilane (1,4-PA-APTS). To a solution of terephthaloyl dichloride (1,4-PACl, 2.05 g, 10 mmol) in 25 mL of dry toluene, a mixture of APTS (4.9 mL, 21 mmol) and triethylamine (14 mL, 100 mmol) in 20 mL of toluene was slowly added. The reaction was stirred at room temperature overnight. The reaction mixture was then filtrated and the solvent was removed under reduced pressure. The final product was a light yellow solid. Yield: 5.02 g (88%). ^1H NMR (DMSO-d_6) δ: 8.58 (br, 2H, NH^{APTS}), 7.90 (s, 4H, aromatic), 3.75 (q, 12H, CH_2–OSi^{APTS}), 3.25 (q, 4H, CH_2–NH^{APTS}), 1.58 (m, 4H, CH_2–CH_2^{APTS}), 1.14 (t, 18H, CH_3^{APTS}), 0.59 (t, 4H, CH_2–Si^{APTS}). $^{13}C\{^1H\}$ NMR (DMSO-d_6) δ: 165.4 (C=O), 136.7 (1,4-aromatic), 127.0 (2,3,5,6-aromatic), 57.7 (CH_2–O–Si^{APTS}), 42.1 (CH_2–NH^{APTS}), 22.7 (CH_2–CH_2^{APTS}), 18.2 (CH_3^{APTS}), 7.5 (CH_2–Si^{APTS}). Elemental Anal. Calc. for $C_{26}H_{48}N_2O_8Si_2$: C, 54.51; H, 8.45; N, 4.89%. Found: C, 54.28; H, 8.42; N, 4.88%.

Synthesis of *N,N*-dioctyl-1,2-phthaloyl diamido (1,2-DOPA). The 1,2-DOPA ligand was synthesized via the Schotten-Baumann approach.[25] A solution of 1,2-PACl (0.77 mL, 5 mmol) in Et_2O (30 mL) was added dropwise to a solution of *N,N*-dioctylamine (3.3 mL, 10.5 mmol) and NaOH (1.2 g, 30 mmol) in water (36 mL) at room temperature over 30 min. The reaction was stirred overnight and the phases were separated. The aqueous layer was saturated with NaCl and extracted with Et_2O (3 × 30 mL), and the combined organic layers were washed with an aqueous solution of 10% HCl (3 × 20 mL). The organic layer was washed again with water, and then dried over $MgSO_4$. The solvent was removed under reduced pressure, yielding a light-yellow oil as final product. Yield: 3.68 (69%). ^1H NMR (*chloroform-d*) δ: 7.32 (m, 2H, 3,6-aromatics), 7.23 (m, 2H, 4,5-aromatics), 3.35 (dt, 8H, CH_2–Noctyl), 1.58 (d, 8H, CH_2–CH_3^{octyl}), 1.29 (td, 40H, CH_2^{octyl}), 0.82 (t, 12H, CH_3^{octyl}). $^{13}C\{^1H\}$ NMR (*chloroform-d*) δ: 169.8 (s, C=O), 135.0 (s, 1,2-aromatics), 128.3 (s, 3,6-aromatis), 126.2 (s, 4,5-aromatics), 45.2 (d, CH_2N), 31.9, 29.4, 29.2, 28.6, 27.6, 27.3, 26.7 (CH_2), 22.8 (s, CH_2–CH_3), 14.2 (s, CH_3). Elemental Anal. Calc. for $C_{40}H_{72}N_2O_2$: C, 78.37; H, 11.84; N, 4.57%. Found: C, 78.59; H, 11.84; N, 4.58%.

Synthesis of *N,N*-dioctyl-1,3-phthaloyl diamido (1,3-DOPA). The compound was synthesized in a similar manner to the method mentioned above. The synthesis conditions were as follows: 1,3-PACl (1.04 g, 5 mmol), *N,N*-dioctylamine (3.3 mL, 10.5 mmol), and NaOH (1.2 g, 30 mmol). Yield: 2.52 g (70%). ^1H NMR (*chloroform-d*) δ: 7.33 (m, 3H, 4,5,6-aromatics), 7.28 (m, 1H, 2-aromatic), 3.42 (dt, 8H, CH_2–N^{octyl}), 1.59 (d, 8H, CH_2–CH_3^{octyl}), 1.23 (td, 40H, CH_2^{octyl}), 0.83 (t, 12H, CH_3^{octyl}). $^{13}C\{^1H\}$ NMR (*chloroform-d*) δ: 170.8 (s, C=O), 137.4 (s, 1,3-aromatics), 127.2 (s, 2-aromatic), 127.2 (s, 4,6-aromatics), 124.7 (s, 5-aromatic), 49.1 (d, CH_2N), 31.8, 29.2, 28.7, 27.5, 27.1, 26.6 (CH_2), 22.6 (s, CH_2–CH_3), 14.1 (s, CH_3). Elemental Anal. Calc. for $C_{40}H_{72}N_2O_2$: C, 78.37; H, 11.84; N, 4.57%. Found: C, 78.47; H, 11.87; N, 4.57%.

Synthesis of *N,N*-dioctyl-1,4-phthaloyl diamido (1,4-DOPA). This compound was synthesized in a similar manner to the method mentioned above. The synthesis conditions were as follows: 1,4-PACl (1.03 g, 5 mmol), *N,N*-dioctylamine (3.3 mL, 10.5 mmol), and NaOH (1.2 g, 30 mmol). Yield: 2.29 g (63%). ^1H NMR (*chloroform-d*) δ: 7.35 (s, 4H, aromatics), 3.45 (dt, 8H, CH_2–N^{octyl}), 1.63 (d, 8H, CH_2–CH_3^{octyl}), 1.27 (td, 40H, CH_2^{octyl}), 0.85 (t, 12H, CH_3^{octyl}). $^{13}C\{^1H\}$ NMR (*chloroform-d*) δ: 171.0 (s, C=O), 138.1 (s, 1,4-aromatics), 127.0 (s, 2,3,5,6-aromatics), 49.1 (d, CH_2N), 31.9, 29.4, 28.9, 27.6, 27.2, 26.7 (CH_2), 22.7 (s, CH_2–CH_3), 14.2 (s, CH_3). Elemental Anal. Calc. for $C_{40}H_{72}N_2O_2$: C, 78.37; H, 11.84; N, 4.57%. Found: C, 78.59; H, 11.85; N, 4.58%.

Synthesis of KIT-6 silica. KIT-6 silica materials were obtained following the procedure reported by Kleitz et al.[26] Briefly, Pluronic P123 ($EO_{20}PO_{70}EO_{20}$) (9.0 g) was dissolved in distilled water (325.0 g), and HCl (37%) (17.4 g) was added under vigorous stirring. After complete dissolution, *n*-butanol (BuOH) (9.0 g) was added. The reaction mixture was left under stirring at 35 °C for 6 h, after which tetraethoxysilane (TEOS) (19.4 g) was added at once to the homogenous solution. The molar composition of the starting mixture was TEOS/P123/HCl/H_2O/BuOH = 1.0/0.017/1.83/195/1.31. This mixture was left under stirring at 35 °C for 24 h, followed by an aging step at 100 °C for 24 h under static conditions. The resulting solid product was then filtered and dried for 24 h at 100 °C. From the as-synthesized KIT-6 material, the template was removed by extraction in ethanol-HCl mixture, followed by calcination in air at 550 °C for 5 h.

Materials functionalization. Prior to the grafting procedure, the KIT-6 support was activated overnight at 150 °C under vacuum. To functionalize KIT-6, 1.0 g of the support materials was dispersed in 60 mL of dry toluene under inert atmosphere. After 20 min, the chosen silane-modified ligand (0.46 g of 1,2/1,3/1,4-PA-APTS) and triethylamine (1.2 mL) were added at once to the suspension. The resulting mixture was stirred under reflux conditions for 24 h. After the modification procedure, the functionalized silica product was filtered and washed thoroughly with toluene. Unreacted silane molecules were removed by Soxhlet extraction in dichloromethane for at least 12 h. The resulting products are noted as KIT-6-1,2-PA, KIT-6-1,3-PA, and KIT-6-1,4-PA, respectively.

Characterization techniques. N_2 adsorption-desorption isotherms were measured at -196 °C (77 K) using an Autosorb-1-MP sorption analyzer (Quantachrome Instruments, Boynton Beach, Fl, USA). Prior to the analysis, the samples were outgassed for at least 12 h at 200 °C (unmodified KIT-6) or at 80 °C (functionalized sorbents) under turbomolecular pump vacuum.

The specific surface area (S_{BET}) was determined using the Brunauer-Emmett-Teller equation in the relative pressure range 0.05 ≤ P/P_o ≤ 0.20 and the total pore volume (V_{pore}) was measured at P/P_o = 0.95. The pore size distributions were calculated using the nonlocal density functional theory (NLDFT) method (Autosorb-1 software) considering the sorption of nitrogen at -196 °C in silica with cylindrical pores. The pore widths were determined by applying the NLDFT kernel of equilibrium isotherms (desorption branch). FTIR spectra were recorded using a Nicolet Magna FTIR spectrometer with a narrow band MCT detector (Specac Ltd., London). Spectra were obtained from 64 scans with a 4 cm^{-1} resolution. Simultaneous thermogravimetric analysis-differential thermal analysis (TGA/DTA) was performed using a Netzsch STA 449C thermogravimetric analyzer, under air flow of 20 mL min^{-1}. The analysis was performed with a heating rate of 10 °C min^{-1} and a protective nitrogen flow rate of 20 mL min^{-1} from 35 to 700 °C. The low-angle powder X-ray diffraction (XRD) patterns were recorded on a Rigaku Multiplex instrument operated at 2 kW, using Cu Kα radiation (KAIST, Daejeon, Republic of Korea). XRD scanning was performed under ambient conditions in steps of 0.01, with an accumulation time of 0.5 s. Elemental analysis was performed by the combustion method using a CHNS Analyzer Flash 2000, Thermo Scientifc. ^{29}Si magic-angle-spinning (MAS) and ^{13}C cross-polarization (CP/MAS) nuclear magnetic resonance (NMR) analyses were carried out on a Bruker Avance 300 MHz spectrometer (Bruker Biospin Ltd, Milton, Canada) at 59.6 MHz for ^{29}Si and 75.4 MHz for ^{13}C. ^{29}Si MAS NMR spectra were recorded with a spin echo sequence to avoid instrument background with a recycle delay of 30 s in a 4 mm rotor spin at 9 kHz. ^{13}C CP/MAS NMR spectra were recorded with a 4 mm MAS probe with a spinning rate of 9 kHz and contact time of 1 ms. Chemical shifts were referenced to tetramethylsilane (TMS) for ^{29}Si and adamantane for ^{13}C. All the synthesized ligands were characterized by ^{1}H and ^{13}C liquid NMR (see Figures S1-S12). The liquid NMR spectra were recorded on a Varian Inova NMR AS400 spectrometer at 400.0 MHz (^{1}H) and 100.580 MHz (^{13}C). ^{1}H NMR and $^{13}C\{^{1}H\}$ NMR chemical shifts are referenced to residual protons or carbons in deuterated solvent.

Extraction methodology. Extraction behavior of REEs and additional metals was investigated on unfunctionalized KIT-6 and 1,2-PA-APTS, 1,3-PA-APTS, and 1,4-PA-APTS functionalized mesoporous silica. Extraction experiments were performed either as a solid-phase batch extraction (SPE) or flow-through mode. Liquid-liquid extraction (LLE) experiments were also performed in order to determine the effect of ligand grafting on the extractive properties. Elemental quantification of the various elements was performed by ICP-MS/MS (Model 8800, Agilent Technologies) measurement. The initial and final concentrations of the REEs and additional metals in solutions were determined and used to calculate either extraction capacity or distribution constant (K_d, mL g^{-1}) by the following equation:

$$K_d = \frac{V}{m} \times \frac{C_0 - C_f}{C_f} \quad (1)$$

where V is the volume (mL) of the testing solution, m is the amount of the sorbents (mg), C_o and C_f are the initial and final concentration of the REEs (μg L^{-1}), respectively.

Solid-phase batch extraction studies. Prior to the analysis, the functionalized materials (sorbents) were outgassed at 80 °C overnight. Typical batch solid-phase extraction (SPE) experiments of REE solution with functionalized mesoporous KIT-6 was carried out in a 10 mL centrifuge tube, where solutions of REEs (Y, La, Ce, Pr, Nd, Sm, Eu, Gd, Tb, Dy, Ho, Er, Tm, Yb, Lu) and additional ions (Al and Fe) in diluted HNO_3 (pH = 4) were prepared in the desired concentration, *i.e.*, 15 μg L^{-1} for unfunctionalized KIT-6 and 30 μg L^{-1} for functionalized KIT-6. For each sample, 10 mg of sorbents was dispersed in 5 mL of REEs solution (solution/solid ratio was fixed to 500 mL g^{-1}). Only the average values of triplicates are given. After adsorption for 2 h, the supernatant was filtered through a 0.2 μm syringe filter. An Indium (In) solution (50 μg L^{-1}) in 4% HNO_3 was used as internal standard in order to correct the instrumental drift and matrix effects during analysis.

pH variation studies. The pH tests were performed using a solution of REEs (50 μg L^{-1}) prepared at various pH (from 2.5 to 6.2). The pH was adjusted by diluted NH_4OH or HNO_3 solution. For clarity, only the ions with the highest K_d value were shown in this study, and the amount of ion adsorbed on the sorbents at equilibrium was calculated by the following equation:

$$Q_e = \frac{V}{m} \times (C_0 - C_f) \quad (2)$$

All samples were analyzed in triplicates using the batch extraction protocol mentioned above and only the average value was presented.

Adsorption kinetics studies. The kinetic studies were performed for the pristine KIT-6 and KIT-6-1,2-PA. A solution of 40 mg L^{-1} and 0.4 mg L^{-1} of Lu^{3+} was used for KIT-6-1,2-PA and KIT-6, respectively, and the pH was adjusted to 4. The contact time was varied from 1 min to 2 h.

Adsorption isotherm studies. The isotherm studies were performed for the pristine KIT-6 and KIT-6-1,2-PA. Solutions of Lu^{3+} with concentration ranging from 0.1 to 0.9 mg L^{-1} for KIT-6 and 5 to 100 mg L^{-1} for KIT-6-1,2-PA were used. For all solutions, pH was adjusted to 4. The contact time was 2 h.

Liquid-liquid extraction (LLE) studies. 25 μmol of 1,2-DOPA, 1,3-DOPA, or 1,4-DOPA was added to 5 mL of dichloromethane or dodecane, whereas 3 M nitric acid containing 100 μg L^{-1} of each REE was prepared from a standard solution by appropriate dilution, and used as aqueous phase. Both phases (5 mL each) were mechanically mixed for 90 min. The two phases were then separated and the elemental quantification of the REEs in

aqueous phase was performed by ICP-MS/MS. The distribution constant (K_d) for liquid-liquid extraction is calculated by the following equation:

$$K_d = \frac{C_{org}}{C_{aq}} \quad (3)$$

where C_{org} and C_{aq} represent the final concentration of REEs (µg L^{-1}) after extraction.

Reusability tests. 20 mg of KIT-6-1,2-PA mesoporous sorbents were packed inside a 2 mL cartridge (Eichrom Technologies, USA) using the slurry-packing technique described elsewhere.[14] Prior to the loading of extraction solution, the column was washed with high purity water (10 mL) and conditioned with 10 mL of diluted HNO_3 (pH = 4). The solution of extraction (Lu^{3+}, 100 µg L^{-1}, 5 mL) was passed through the column using a peristaltic pump (Minipuls 3, Gilson, USA) with fixed volumetric flow rate of 1 mL min^{-1}. The retained element was eluted from the column with 5 mL of 0.1 M solution of ammonium oxalate ($(NH_4)_2C_2O_4$). Afterwards, the columns were washed with nanopure water (10 mL), reconditioned with HNO_3 (pH = 4) and used for the second extraction. The above-mentioned procedure was repeated 10 times.

Application to real-world samples. Two samples released from mining sites were obtained from industrial partners and analyzed by ICP-MS/MS before and after extraction. The samples were pretreated after acid leaching from mineral deposits of silicate (denoted by IS-1) or niobium (Niobec, Saint-Honoré, QC, Canada, denoted by IS-2) and are preserved with 6 M HCl. Prior to extraction test, the solutions were diluted 1,000 times to ensure that the concentration of REEs in the dilution was 10,000 – 1 µg L^{-1}. The pH of the samples was adjusted to 4.0 using diluted NH_4OH. The extraction procedure used was the same as mentioned in the batch SPE studies.

3. RESULTS AND DISCUSSION

Synthesis and characterization of the materials

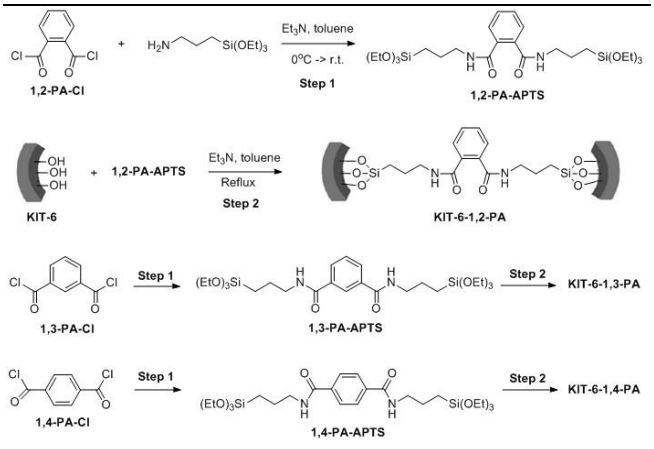


Figure 1. Schematic representation of the synthesis of phthaloylamide-functionalized KIT-6 materials.

The 1,2/1,3/1,4-PA-APTS ligands were synthesized by modification of corresponding acid chlorides with 3-aminopropyltriethoxysilane (APTS) in good yield. The post-synthesis modification of the mesoporous KIT-6 silica support was performed with the appropriate amount of ligand according to a standard one-step procedure in dry toluene under reflux conditions, as schematized in Figure 1. The resulting surface-modified OMS were assigned the respective codes: KIT-6-1,2-PA, KIT-6-1,3-PA, and KIT-6-1,4-PA. The low angle powder XRD patterns of the functionalized materials show well-resolved diffraction peaks corresponding to *Ia3d* symmetry, as expected for KIT-6 derived materials (Figure S13).[14,26] The N_2 physisorption analysis isotherms are presented in Figure 2, and the physicochemical parameters (porosity and structural parameters) derived from the N_2 sorption analysis are compiled in Table 1. All modified materials demonstrate typical type IV isotherms (Figure 2(a)). A steep capillary condensation step and a hysteresis loop (type H1 adsorption–desorption hysteresis) were observed in the relative pressure range (P/P_o) of 0.6–0.8, a characteristic profile for mesoporous solids with large cylindrical mesopores (> 4 nm).[27] After the anchoring of the organic ligands on the silica surface, the shape of the hysteresis loop is well maintained comparing to pristine mesoporous KIT-6. The hysteresis loop shifts to lower values of relative pressure, indicating a decrease in pore size upon surface modification, which is consistent with the pore size distribution (Figure 2(b)). A similar gradual decrease in pore volume compared to the parent silica is observed (Table 1). In all cases, the hysteresis loop and the pore size distribution of modified materials remain narrow, which indicates the homogeneous surface functionalization and the absence of pore blocking.

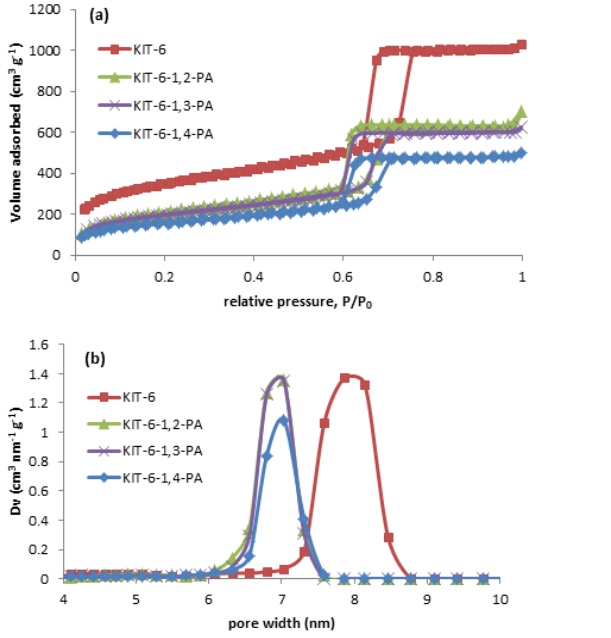


Figure 2. N_2 adsorption–desorption isotherms at -196 °C for the synthesized materials (a) and respective pore size distributions calculated from the desorption branch using the NLDFT method (silica with cylindrical pore model) (b).

Table 1. Physicochemical parameters derived from N_2 physisorption measurements at -196 °C.

Materials	S_{BET} ($m^2\ g^{-1}$)	V_{pore} ($cm^3\ g^{-1}$)	Pore size (nm)
KIT-6	1256	1.52	7.9
KIT-6-1,2-PA	726	1.04	7.0
KIT-6-1,3-PA	712	0.91	7.0
KIT-6-1,4-PA	563	0.72	7.0

To confirm the covalent attachment and the chemical stability of the organic functional groups on the prepared hybrid materials, FT-IR, solid-state NMR, and thermogravimetric analysis (TGA) measurements were performed. As shown in Figure S14, the new characteristic bands in the FT-IR spectra of modified-KIT-6 observed between 1500 and 1700 cm^{-1} can be assigned to the stretching vibration of C=C groups of the aromatic ring from the grafted PA groups, while the wide bands around 3050 cm^{-1} are typical of the stretching vibrations of C–H groups. Moreover, the presence of the amide bond in the modified hybrid solids was confirmed by the characteristic bands visible between 1710 and 1650 cm^{-1} (C=O stretching), and 1520 cm^{-1} (NH bend in amine I) in the FT-IR spectra (Figure S14). These peaks clearly indicate the successful introduction of phthaloyl amide groups into the mesoporous silica. The structure of the anchored ligands was further established by solid-state NMR spectroscopy. The solid-state ^{13}C CP/MAS NMR spectra of PA ligand-functionalized KIT-6 are shown in Figure S15(a). The peaks corresponding to the ligands were clearly defined in the ^{13}C CP/NMR spectra and were in good accordance with those observed in the liquid ^{13}C NMR spectra of the APTS-modified ligands in DMSO-d_6 (Figure S2-S6). Three intense peaks can be observed at chemical shifts δ = 8.9, 22.4, and 42.5, which can be assigned to methylene carbon atoms from the silicon to the nitrogen ends in the (–Si–CH_2–CH_2–CH_2–N–) chain (carbon atoms no. 1–3, respectively, Figure S15 (a)). The peaks in the δ range of 120–150 can be assigned to the aromatic carbon atoms of the phthaloyl moiety, while the band appearing at 170 ppm is characteristic of the carbonyl group. Besides, it is noted that two additional peaks assigned to ethoxy groups in (–Si–O–CH_2–CH_3) appears at δ = 60 and 16 (carbon r and r', respectively), which suggests that a small portion of the ethoxysilane species remained unreacted during the functionalization. However, it is worth noticing that these peaks are much less pronounced compared to those in the liquid state NMR, indicating that their concentration on the silica surface can be considered relatively low. Indeed, as shown on the ^{29}Si MAS NMR spectra (Figure S15(b)), for KIT-6-1,2-PA and KIT-6-1,3-PA, the ligands have been anchored to the silica support mostly through T^2 ($(SiO)_2(OR)Si$-R) and T^3 ($(SiO)_3Si$-R) species at -60 and -68 ppm, respectively, whereas a part of 1,4-PA-APTS attaches to KIT-6 through T^1 ($(SiO)(OR)_2Si$–R) at -50 ppm. This further confirms that the organic ligands are covalently anchored to the surface through grafting on silanol groups,[28,29] thus are less prone to leaching upon extraction, and provide a certain rigidity and stability to the hybrid materials.

Table 2. Total amount of ligand introduced by grafting for the different functionalized materials and estimated surface density of the ligands.

Materials	Mass loss[a] (%)	CHN (%)		Density of ligand[b] (nm^{-2})
		N	C	
KIT-6-1,2-PA	16.7	1.68	10.35	0.32
KIT-6-1,3-PA	17.1	1.74	11.45	0.35
KIT-6-1,4-PA	17.8	1.62	11.30	0.43

[a.] Determined by TGA-DTA analysis in temperature range 140 - 650 °C. [b.] Calculated using N content from CHN analysis and specific surface area (S_{BET}, Table 1).

In addition, the composition of the organic moieties attached to the silica surface was evaluated using TGA and CHN elemental analysis. Reasonable ligand loading was achieved for all mesoporous KIT-6 materials (Table 2). The TGA and DTA profiles of functionalized materials indicate that the ligands follow either a two-step (KIT-6-1,2-PA) or a three-step (KIT-6-1,3-PA and KIT-6-1,4-PA) degradation, and the pyrolysis process of the organic moieties begins between 120 and 140 °C, indicating that the ligands are covalently attached on the mesoporous silica support (Figure S16). The higher loading of ligand for KIT-6-1,4-PA is probably due to the *para* positioning, which renders the grafting of both sides of the ethoxysilane groups more difficult, thus reducing the surface area (S_{BET}) and pore volume while maintaining the pore size (Table 1). The higher ratio of T_1 peak for KIT-6-1,4-PA compared to KIT-6-1,2-PA and KIT-6-1,3-PA on the ^{29}Si MAS NMR spectra further confirms this suggestion. Based on the data obtained from the N_2 physisorption at -196 °C and the amounts of carbon and nitrogen on the hybrid materials obtained from elemental analysis, the apparent surface density of the ligands was also calculated (Table 2). The highest apparent surface density was estimated for KIT-6-1,4-PA (0.43 nm^{-2}), while the lowest surface density of ligand was found for the sorbent KIT-6-1,2-PA (0.32 nm^{-2}), which is in agreement with the TGA mass loss and surface area observed for the functionalized materials. Note that the surface density of ligands, however, is slightly overestimated since the unreacted ethoxyl groups also contribute to the weight loss in the pyrolysis temperature range.

Extraction studies

Effect of pH. The H^+ ions in the solution can strongly affect the uptake of metal ions by the adsorbents. Herein, the effect of pH (ranging from 2.5 to 6.2) on functionalized sorbents was investigated using a mixture of REEs

(50 µg L^{-1}). For clarity, only the ions with the highest K_d values (*i.e.*, Lu, Sm, and Ce for KIT-6-1,2-PA, KIT-6-1,3-PA, and KIT-6-1,4-PA, respectively; see below) are shown on Figure 3. It is clear that the REEs adsorption capacity of the functionalized sorbents increases rapidly with augmentation of the solution pH. At lower pH (pH 2.5), the H^+ can compete with metal ions in the complexation with functional moieties and positively charges the surface of the sorbents, resulting in electrostatic repulsion between the REEs ions and silica surface. At higher pH (pH ≥ 7), however, the REEs tend to precipitate as hydroxides. As shown in Figure 3, a pH around 4 enhances the adsorption capacities of sorbents and thus was selected for further sorption experiments.

Extraction performance. The adsorption performance was evaluated using the distribution coefficient (K_d, mL g^{-1}) calculated according to equation (1):

$$K_d = \frac{V}{m} \times \frac{C_0 - C_f}{C_f} \quad (1)$$

and the effect of ligand grafting on the REEs extraction is shown in the Figure 4 and Table S2. It is clearly observable that the grafting of ligand 1,2-PA-APTS, 1,3-PA-APTS, and 1,4-PA-APTS results in a significantly higher extraction capacity as compared to pristine KIT-6. The selectivity pattern is also different according to the nature of the tethered organic ligands. The extraction selectivity of the hybrid materials is supposed to stem from the synergistic effects of the chelating angle (*bite angle*) of organic moieties and the silica surface,

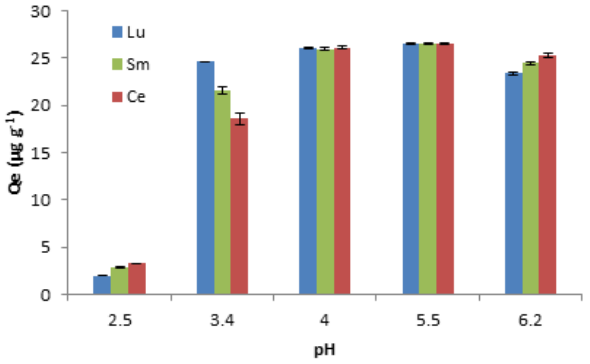


Figure 3. Effect of pH on the REEs adsorption by functionalized KIT-6 sorbents (Lu for KIT-6-12,-PA, Sm for KIT-6-1,3-PA, and Ce for KIT-6-1,4-PA).

which can also act as a ligand, thus forming a multidentate coordination cavity for REEs. Among the three ligands, the 1,2-PA-APTS exhibits the smallest *bite angle* and will form a smaller cavity. As such, this material shows an impressive affinity towards late lanthanides such as Ho, Er, Tm, Yb, and Lu, with K_d values higher than 10 000 mL g^{-1}. It is worth noticing that the K_d value of Y^{3+} (12 400 mL g^{-1}) is almost as high as that of Ho^{3+} (11 700 mL g^{-1}), which can be explained by the similarity in their ion radius (90 pm and 90.1 pm for Y^{3+} and Ho^{3+}, respectively). In case of the KIT-6-1,3-PA material, with a larger cavity, a well-defined selectivity towards large-/middle-size lanthanides, namely Ce^{3+} (101 pm), Pr^{3+} (99 pm), Nd^{3+} (98 pm), and Sm^{3+} (97 pm), was observed. This observation is consistent with the relative larger *bite angle* of 1,3-PA-APTS compared to 1,2-PA-APTS, which favors the complexation with lanthanides bearing larger ion radii. It should be noted that the highest K_d value of KIT-6-1,3-PA (22 700 mL g^{-1} for Nd^{3+}) is lower than that of KIT-6-1,2-PA (53 500 mL g^{-1} for Lu^{3+}), which is probably due to the presence of the hydrogen atom in the position 2 of the aromatic ring in 1,3-PA-APTS, which should adversely influence the complexation of the carbonyl groups with REEs ions. Finally, in the case of KIT-6-1,4-PA, although the general extraction capacity was enhanced compared to the pristine KIT-6 sample, the hybrid material shows only small perturbation in the K_d values through the lanthanide series and exhibits little selectivity compared to its KIT-6-1,2-PA and KIT-6-1,3-PA counterparts, as expected. Here, the two carbonyl groups being in *para* position prevent any synergistic action of the moieties which could lead to efficient sorption of lanthanides.

To determine the effect of ligand grafting on the extraction performance, the LLE experiments were also performed for 1,2-DOPA, 1,3-DOPA, and 1,4-DOPA. It is observed that, under the conditions tested (100 µg L^{-1} of REE in 3 M HNO_3), the K_d values for LLE are relatively small, showing limited extraction capacity (Figure S17). Beside the long carbon chains which induce hydrophobicity of the molecules, a more rigid frame (the aromatic ring) further renders the molecules less hydrophilic (thus the lack of solubility in dodecane) and decrease the extraction yield in LLE, whereas the use of solid support eliminates this effect. Furthermore, contrary to its SPE counterparts among which each demonstrates distinctive selectivity, the K_d values for all of the three ligands showed little variation across the lanthanides. The striking difference in extraction behavior between SPE

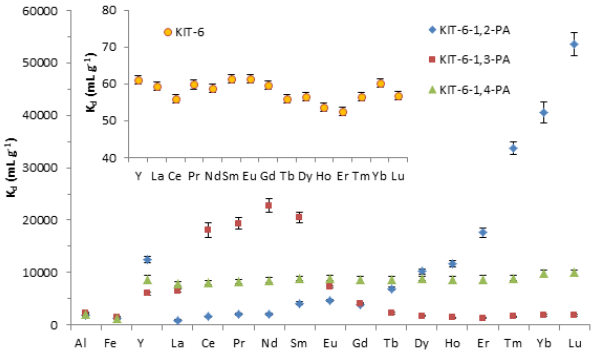


Figure 4. Distribution coefficient (K_d) values for functionalized hybrid materials in the presence of competitive ions (Al^{3+} and Fe^{3+}). For comparison, the K_d value for pristine KIT-6 silica is shown (insert Figure).

and LLE stems from the chemical anchoring of the ligands to the solid surface, which decreases the flexibility of the chelating carbonyl groups and further increases the

overall rigidity of the ligand. Upon grafting, each chelating ligands forms a cavity with the silica surface, in which only those metal ions that fit with the size of the cavity (*i.e.*, having an appropriate ion radius for the *bite angle* of the ligand) will be trapped, whereas the unfitted ions will easily be eluted. These observations further demonstrate the necessity of ligand grafting in enhancing the overall extraction performance of the hybrid sorbents.

The effect of competing ions in the effluent on the uptake of REEs was also investigated. As shown in Figure 4, the K_d values of both Al^{3+} and Fe^{3+} for all three adsorbents are relatively low (< 2000 mL g^{-1}) compared to that of REEs.

Because the KIT-6-1,2-PA shows exceptionally high K_d values, as well as the greatest selectivity towards late lanthanides, it was chosen as a model material for the following studies.

Kinetics studies. To further explore the sorption behavior of REEs on the hybrid KIT-6-PA sorbents and to determine the rate-controlling mechanism during the adsorption, sorption kinetics studies were carried out. The Lu^{3+} ion sorption onto KIT-6-1,2-PA and KIT-6 over a time range of 2 - 120 min was performed, with an initial Lu^{3+} concentration of 40 mg L^{-1} and 0.4 mg L^{-1} for KIT-6-1,2-PA and KIT-6, respectively. As shown in Figure 5, the adsorption of Lu ions by KIT-6-1,2-PA increases fast within the first 10 min of contact, then equilibrium was reached after 45 min of contact. The kinetic curve of pure KIT-6 silica shows no apparent change after 20 minutes due to poor adsorption performance. KIT-6-1,2-PA displays significantly higher adsorption capacity at equilibrium, indicating superior affinity between Lu ions and the adsorbent surface.

To further investigate the nature of extraction behavior, the kinetic curves of KIT-6 and KIT-6-1,2-PA were fitted with pseudo-first-order and pseudo-second order kinetic models. The detailed description of the two models is presented in Supporting Information and the fitting results are shown in Figure 5 and Table 3. According to correlation coefficient R^2, the pseudo-second-order model, which is frequently associated with chemical sorption mechanism,[30,31] gives a better fit for the adsorption data of both KIT-6 and KIT-6-1,2-PA. The Q_e

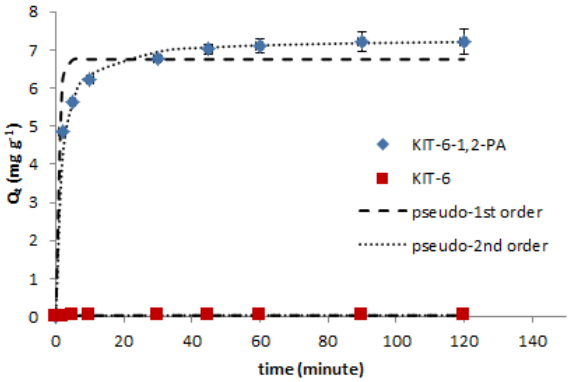


Figure 5. Effect of the contact time on the lutetium sorption with kinetic model fitting of the pseudo-first and -second-order model of the lutetium adsorption kinetic on KIT-6-1,2-PA and KIT-6 at room temperature.

values calculated from the pseudo-second-order model for both KIT-6 and KIT-6-1,2-PA sorbents are also in good agreement with experimental data $Q_{e,exp}$ (Table 3). The adsorption curve and kinetic model fitting suggest that the uptake of Lu ion is carried out in two successive steps: (1) rapid surface adsorption associated with ion diffusion, followed by (2) chemical sorption of ions contributed by functional groups on the surface, between which the chemisorption process being the rate-limiting step of the sorption mechanism.

Adsorption isotherm. Equilibrium adsorption experiments were carried out to calculate the maximum of adsorption capacity of the material KIT-6-1,2-PA. The study was performed at pH 4, with 10 mg of sorbent, 5 mL of solution, and 2 h equilibrium time. The detailed description of the experiment can be found in the Experimental Section and Supporting Information. As shown in Figure 6, the adsorption capacities of KIT-6-1,2-PA and KIT-6 are non-linear and increase with an increase of the initial concentration of Lu^{3+} (from 5 to 100 mg L^{-1} for KIT-6-1,2-PA and from 0.1 to 0.9 mg L^{-1} for KIT-6). Both Langmuir and Freundlich isotherm model were applied to describe the adsorption mechanism and the Langmuir model gives a better fit (R^2 > 0.99), suggesting homogenous binding sites on the surface of sorbents,[32] which results in finite molecular sorption. The linear regression of the Langmuir model is shown in the Figure S19 with the parameters compiled in the Table S1. The experimental maximum adsorption capacity for KIT-6-1,2-PA is found to be 8.57 mg g^{-1}, which is in good agreement with equilibrium adsorption capacity calculated by the Langmuir model Q_m (8.69 mg g^{-1}). Further, the maximum adsorption capacity of KIT-6-1,2-PA is much higher than that of pristine KIT-6 (Q_m = 0.0598 mg g^{-1} calculated by Langmuir model) at the same pH (pH = 4), demonstrating an outstanding adsorption capacity. This result is also consistent with the much higher K_d value for KIT-6-1,2-PA compared to pristine KIT-6 (Figure 4). In addition, in the Langmuir isotherm model, the separation factor R_L is found to be 0.0164 and 0.0181 for KIT-6-1,2-PA and KIT-6, respectively (Table S1). The R_L indicates if the adsorption is favorable (0 < R_L < 1), unfavorable (R_L > 1), linear (R_L = 1), or irreversible (R_L =0); the smaller the R_L value is, the more favorable the sorption on the sorbent is for the given ion. The smaller R_L value of KIT-6-1,2-PA thus further confirms that KIT-6-1,2-PA is

Table 3. Kinetic constants for the pseudo-first-order and pseudo-second-order models.

Materials	Kinetics model							
		Pseudo-first-order			Pseudo-second-order			
	$Q_{e,exp}$ (mg g^{-1})	$Q_{e,cal}$ (mg g^{-1})	k_1 (L min^{-1})	R^2	$Q_{e,cal}$ (mg g^{-1})	k_2 (g mg^{-1} min^{-1})	$t_{1/2}$ (min)	R^2
KIT-6-1,2-PA	7.31	6.75	1.25	0.938	7.30	0.0909	1.51	0.999
KIT-6	0.0368	0.0359	0.251	0.967	0.0370	15.07	1.79	0.999

more favorable in sorption of Lu^{3+} than KIT-6. Although in this work the Q_m value for Lu^{3+} appears to be lower than those reported in the literature under similar conditions,[19] it is worth noting that the same geometric parameters cannot be used to compare a tri/tetradentate ligand with a bidentate ligand, as in this case. Higher or similar extraction capacity was obtained for lanthanides using other systems such as mesoporous polymers networks[33–35], ion-exchangers,[36,37] and magnetic nanosorbents.[38,39] However, these systems require laborious or multi-step synthesis and purification, whereas in this work all the ligands can be obtained using one-step synthesis from commercially available starting materials without further chromatographic purification, followed by simple, one-step grafting procedure to obtained the functionalized sorbents. Moreover, the amount of ligand grafted on the surface in this work (around 17%) is significantly lower than what has been previously reported (more than 27% for most of the cases).[11,19,34] Therefore, a scale-up can easily overcome this minor drawback.

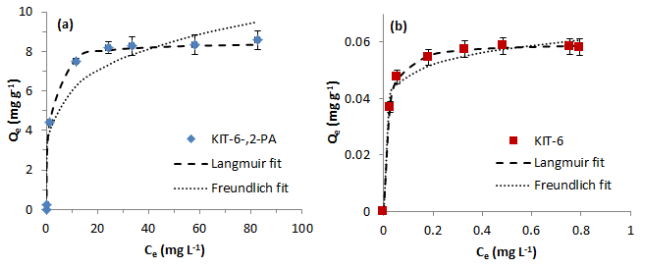


Figure 6. Experimental equilibrium isotherm data and modeling for the adsorption of Lu^{3+} on mesoporous silica KIT-6-1,2-PA (a) and KIT-6 (b).

Stripping and reusability tests. To evaluate the reusability of the functionalized mesoporous materials, a SPE cartridge was packed using KIT-6-1,2-PA,[14] and its reusability performance for Lu extraction was assessed (Figure 7). The ICP-MS/MS analysis results showed that no significant loss in Lu extraction efficiency was observed even after 10 loading-stripping-regeneration cycles (98.7% and 94.9% for the first and 10th cycle, respectively). However, since the material demonstrates impressive extraction capacity (distribution coefficient K_d > 50000 mL g^{-1} for lutetium), the possible degradation would not directly impact the overall extraction efficiency of the functionalized materials. The oxalate solution after stripping was also analyzed by ICP-MS/MS, and these results show that the most part of Lu that has been extracted from the initial solution was recovered; the small portion of missing Lu ions is probably released by water during the following washing step and/or by diluted HNO_3 during the reconditioning step.[40]

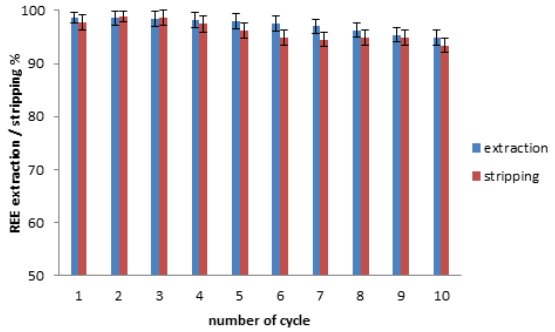


Figure 7. Reusability performance of KIT-6-1,2-PA sorbent over 10 loading-stripping-regeneration cycles, in the dynamic system.

The packed materials were recovered after 10 cycles and fully characterized. The results obtained from N_2 physisorption analysis showed an increase in both surface area (from 726 to 768 m^2 g^{-1}, Figure S20) and in pore size distribution (from 7.0 to 7.3 nm). These phenomena can be explained by the loss (leaching) of some organic moieties attached to the surface of silica. The TGA then confirmed this assumption, showing a small reduction in mass loss between 140 to 700 °C (from 16.7 to 15.5%, Figure S21). Finally, the ^{13}C CP/MAS NMR spectrum showed the decrease in intensity of the peak at 61 ppm and disappearance of the one at 16 ppm, indicating the partial hydrolysis of the grafted ligand, especially the ethoxysilane groups, mostly due to the presence of diluted HNO_3 (Figure S22). This result is in line with the decrease of mass loss. However, the ^{13}C CP/MAS NMR spectrum also demonstrates that the overall ligand structure is well preserved. These results show that in addition to its impressive extraction capacities, the functionalized materials can withstand multiple loading-stripping-regeneration cycles under the conditions tested without significant degradation.

Application to real-world samples. To further demonstrate the applicability of the KIT-6-PA type sorbents for REEs sequestration in real samples, extraction tests were carried out with industrial samples released from silicate (IS-1) or niobium (IS-2) mining deposits provided by industrial partners. Prior to the extraction tests, the stock solutions were diluted 1,000 times to make sure that the concentration of each REE in the dilution was 10,000 – 1 µg L^{-1}. The elemental composition of dilut-

ed samples was analyzed by ICP-MS/MS and is compiled in the Table S4. The extraction tests with real-world

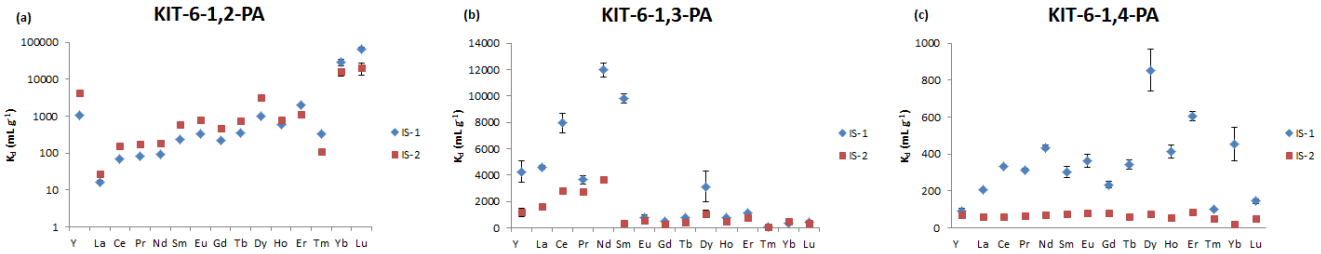


Figure 8. Selectivity of REEs adsorption for KIT-6-1,2-PA (a), KIT-6-1,3-PA (b), and KIT-6-1,4-PA (c) for industrial samples IS-1 and IS-2. For clarity, the K_d values for KIT-6-1,2-PA was presented on a logarithmic scale.

samples are of practical importance as industrial and mining waste is characterized by various competitive ions with high concentration and therefore high ionic strength. Figure 8 shows the K_d values of REEs in IS-1 and IS-2 for functionalized hybrid materials. Compared to batch extraction using standard solutions (30 µg L^{-1} for each REE), industrial samples treatment showed lower K_d values for REEs. Indeed, as shown in the Table S4, both IS-1 and IS-2 consist of complex ion matrix and large amount of competitive metal ions resulting from mining and leaching process, including Na^+, K^+, Fe^{3+}, Al^{3+}, Ca^{2+}, and Mg^{2+}, which are likely to compete with REEs and reduce the affinity between sorbent surface and target ions. Furthermore, the REEs matrix is rich in early lanthanides (La^{3+}, Ce^{3+}, Pr^{3+}, and Nd^{3+}) for both IS-1 and IS-2. Noticeably, distinctive selectivity towards REEs is still observed for KIT-6-1,2-PA (Y, Yb, and Lu) and KIT-6-1,3-PA (Ce, Nd, and Sm), which is similar to the selectivity pattern obtained using standard solution. KIT-6-1,4-PA shows limited extraction capacity and selectivity, as expected. In addition, the interaction of ligands on the silica surface with REEs is strongly favored over competitive ions, as shown on Figure S23. Overall, the results suggest the potential applicability and suitability of the system for REEs recovery from mining and industrial deposits.

4. CONCLUSION AND PERSPECTIVES

In this work, we reported a series of novel, efficient and robust mesoporous sorbents functionalized by phthaloyl diamide (PA) ligands. Three preorganized, chelating ligands with different *bite angles* were successfully grafted on the KIT-6 surface, and size-based selectivity towards REEs was observed in the presence of competitive ions. At pH 4, the synthesized sorbents clearly demonstrate high efficiency with rapid adsorption kinetics (within 1 h) and significant adsorption capacity (8.47 mg g^{-1}). Dynamic extraction tests show that the materials are reusable for up to 10 loading-stripping-regeneration cycles while maintaining the chemical structure of organic moieties. These results are of importance since they clearly demonstrate that the grafting of easily accessible molecular structures, such as the PA ligands, on ordered silica can lead to highly efficient materials for REEs extraction when the homogeneous analogues are more or less inactive. Indeed, the synergistic action of the ligand and the surface leads to an enhanced coordination environment. The extraction of REEs in real-world samples demonstrates the possibility in industrial application of these materials. Future work will emphasize on exploring novel preorganized chelating ligands that might not have good extraction capacity and selectivity in the homogeneous phase but could be efficient when supported, and on the synthesis of functional materials with nanoporous monolithic structures for industrial applications such as dynamic column extraction in high pressure environment.

ASSOCIATED CONTENT

Supporting Information

Supplementary Information (SI) available: Low angle XRD patterns of the materials, ^1H and ^{13}C NMR spectra, ^{13}C cross polarization (CP) and ^{29}Si magic-angle spinning (MAS) NMR spectra, FT-IR spectra, plots of TGA-DTA, linear regression and the corresponding parameters of the kinetics and adsorption isotherm experiments, N_2 sorption isotherms of the KIT-6-1,2-PA materials after reusability tests, and Ln extraction (K_d) of the grafted KIT-6 materials and liquid-liquid extraction.

This material is available free of charge via the Internet at http://pubs.acs.org.

AUTHOR INFORMATION

Corresponding Author

*dominic.larriviere@chm.ulaval.ca

*freddy.kleitz@univie.ac.at

*frederic.fontaine@chm.ulaval.ca

ORCID

Yimu Hu: 0000-0003-2787-4181

Freddy Kleitz: 0000-0001-6769-4180

Frédéric-Georges Fontaine: 0000-0003-3385-0258

Notes

The authors declare no competing financial interest.

ACKNOWLEDGMENT

The authors acknowledge the National Sciences and Engineering Research Council of Canada (NSERC) for the finan-

cial support. NSERC supported this work through a Strategic Project Grant (Grant # STPGP 463032 – 14). We thank Mr. Jongho Han and Prof. Ryong Ryoo (IBS and KAIST, Daejeon, Republic of Korea) for providing the low-angle powder XRD data for the samples. We thank Niobec (Saint-Honoré, QC, Canada) for providing industrial samples.

REFERENCES

(1) Massari, S.; Ruberti, M. Rare Earth Elements as Critical Raw Materials: Focus on International Markets and Future Strategies. *Resour. Policy* **2013**, *38* (1), 36–43.

(2) Binnemans, K.; Jones, P. T.; Blanpain, B.; Van Gerven, T.; Yang, Y.; Walton, A.; Buchert, M. Recycling of Rare Earths: A Critical Review. *J. Clean. Prod.* **2013**, *51*, 1–22.

(3) Hatch, G. P. Dynamics in the Global Market for Rare Earths. *Elements* **2012**, *8* (5), 341–346.

(4) *Critical Materials Strategy;* U.S Department of Energy: Washington, DC, 2010. http://energy.gov/epsa/initiatives/ department-energy-s-critical-materials-strategy.

(5) Moss, R. L.; Tzimas, E.; Willis, P.: Arendorf, J.; Thompson, P.; Chapman, A.; Morley, N.; Sims, E.; Bryson, R.; Pearson, J.; Tercero Espinoza, L.; Marscheider-Weidemann, F.; Soulier, M.; Lüllmann, A.; Sartorius, C.; Ostertag, K. *Critical Metals in the Path towards the Decarbonization of the EU Energy Sector*; European Union: Luxembourg, 2013.

(6) Kanazawa, Y.; Kamitani, M. Rare Earth Minerals and Resources in the World. *J. Alloys Compd.* **2006**, *408–412*, 1339–1343.

(7) Sholl, D. S.; Lively, R. P. Seven Chemical Separations to Change the World. *Nat. News* **2016**, *532* (7600), 435-437.

(8) Florek, J.; Giret, S.; Juère, E.; Larivière, D.; Kleitz, F. Functionalization of Mesoporous Materials for Lanthanide and Actinide Extraction. *Dalton Trans.* **2016**, *45* (38), 14832–14854.

(9) De Vos, D. E.; Dams, M.; Sels, B. F.; Jacobs, P. A. Ordered Mesoporous and Microporous Molecular Sieves Functionalized with Transition Metal Complexes as Catalysts for Selective Organic Transformations. *Chem. Rev.* **2002**, *102* (10), 3615–3640.

(10) Florek, J.; Chalifour, F.; Bilodeau, F.; Larivière, D.; Kleitz, F. Nanostructured Hybrid Materials for the Selective Recovery and Enrichment of Rare Earth Elements. *Adv. Funct. Mater.* **2014**, *24* (18), 2668–2676.

(11) Zheng, X.; Wang, C.; Dai, J.; Shi, W.; Yan, Y. Design of Mesoporous Silica Hybrid Materials as Sorbents for the Selective Recovery of Rare Earth Metals. *J. Mater. Chem. A* **2015**, *3* (19), 10327–10335.

(12) Zheng, X.; Liu, E.; Zhang, F.; Yan, Y.; Pan, J. Efficient Adsorption and Separation of Dysprosium from NdFeB Magnets in An Acidic System by Ion Imprinted Mesoporous Silica Sealed in a Dialysis Bag. *Green Chem.* **2016**, *18* (18), 5031–5040.

(13) Lebed, P. J.; de Souza, K.; Bilodeau, F.; Larivière, D.; Kleitz, F. Phosphonate-functionalized Large Pore 3-D Cubic Mesoporous (KIT-6) Hybrid as Highly Efficient Actinide Extracting Agent. *Chem. Commun.* **2011**, *47* (41), 11525–11527.

(14) Lebed, P. J.; Savoie, J.-D.; Florek, J.; Bilodeau, F.; Larivière, D.; Kleitz, F. Large Pore Mesostructured Organosilica-Phosphonate Hybrids as Highly Efficient and Regenerable Sorbents for Uranium Sequestration. *Chem. Mater.* **2012**, *24* (21), 4166–4176.

(15) Yuan, L.-Y.; Zhu, L.; Xiao, C.-L.; Wu, Q.-Y.; Zhang, N.; Yu, J.-P.; Chai, Z.-F.; Shi, W.-Q. Large-Pore 3D Cubic Mesoporous (KIT-6) Hybrid Bearing a Hard–Soft Donor Combined Ligand for Enhancing U(VI) Capture: An Experimental and Theoretical Investigation. *ACS Appl. Mater. Interfaces* **2017**, *9* (4), 3774–3784.

(16) Juère, E.; Florek, J.; Larivière, D.; Kim, K.; Kleitz, F. Support Effects in Rare Earth Element Separation Using Diglycolamide-functionalized Mesoporous Silica. *New J. Chem.* **2016**, *40*, 4325-4344.

(17) Bogart, J. A.; Lippincott, C. A.; Carroll, P. J.; Schelter, E. J. An Operationally Simple Method for Separating the Rare-Earth Elements Neodymium and Dysprosium. *Angew. Chem. Int. Ed.* **2015**, *54* (28), 8222–8225.

(18) Ivanov, A. S.; Bryantsev, V. S. A Computational Approach to Predicting Ligand Selectivity for the Size-Based Separation of Trivalent Lanthanides. *Eur. J. Inorg. Chem.* **2016**, *2016* (21), 3474–3479.

(19) Florek, J.; Mushtaq, A.; Larivière, D.; Cantin, G.; Fontaine, F.-G.; Kleitz, F. Selective Recovery of Rare Earth Elements Using Chelating Ligands Grafted on Mesoporous Surfaces. *RSC Adv.* **2015**, *5* (126), 103782–103789.

(20) Zhao, X.; Wong, M.; Mao, C.; Trieu, T. X.; Zhang, J.; Feng, P.; Bu, X. Size-Selective Crystallization of Homochiral Camphorate Metal–Organic Frameworks for Lanthanide Separation. *J. Am. Chem. Soc.* **2014**, *136* (36), 12572–12575.

(21) Gao, H. Y.; Peng, W. L.; Meng, P. P.; Feng, X. F.; Li, J. Q.; Wu, H. Q.; Yan, C. S.; Xiong, Y. Y.; Luo, F. Lanthanide separation using size-selective crystallization of Ln-MOFs. *Chem. Commun.* **2017**, *53* (42), 5737–5739.

(22) Bryantsev, V. S.; Hay, B. P. Theoretical prediction of Am(III)/Eu(III) selectivity to aid the design of actinide-lanthanide separation agents. *Dalton Trans.* **2015**, *44* (17), 7935–7942.

(23) Hancock, R. D. The pyridyl group in ligand design for selective metal ion complexation and sensing. *Chem. Soc. Rev.* **2013**, *42* (4), 1500–1524.

(24) Jansone-Popova, S.; Ivanov, A. S.; Bryantsev, V. S.; Sloop, F. V.; Custelcean, R.; Popovs, I.; Dekarske, M. M.; Moyer, B. A. Bis-lactam-1,10-phenanthroline (BLPhen), a New Type of Preorganized Mixed N,O-Donor Ligand That Separates Am(III) over Eu(III) with Exceptionally High Efficiency. *Inorg. Chem.* **2017**, 56 (10), 5911-5917.

(25) Leoncini, A.; Huskens, J.; Verboom, W. Preparation of Diglycolamides via Schotten–Baumann Approach and Direct Amidation of Esters. *Synlett* **2016**, *27* (17), 2463–2466.

(26) Kleitz, F.; Choi, S. H.; Ryoo, R. Cubic *Ia3d* Large Mesoporous Silica: Synthesis and Replication to Platinum Nanowires, Carbon Nanorods and Carbon Nanotubes. *Chem. Commun.* **2003**, 17, 2136–2137.

(27) Neimark, A. V.; Sing, K. S. W.; Thommes, M. In *Handbook of Heterogeneous Catalysis*; Wiley-VCH Verlag GmbH & Co. KGaA, 2008.

(28) Pan, Y.-C.; Wu, H.-Y.; Jheng, G.-L.; Tsai, H.-H. G.; Kao, H.-M. Ordered and Hydrothermally Stable Cubic Periodic Mesoporous Organosilicas with SBA-1 Mesostructures: Synthesis, Characterization, Solid-State NMR Spectroscopy, and DFT Calculations. *J. Phys. Chem. C* **2009**, *113* (7), 2690–2698.

(29) Shigeno, T.; Nagao, M.; Kimura, T.; Kuroda, K. Direct Silylation of a Mesostructured Precursor for Novel Mesoporous Silica KSW-2. *Langmuir* **2002**, *18* (21), 8102–8107.

(30) Ho, Y. S.; McKay, G. Pseudo-Second Order Model for Sorption Processes. *Process Biochem.* **1999**, *34* (5), 451–465.

(31) Plazinski, W.; Dziuba, J.; Rudzinski, W. Modeling of Sorption Kinetics: The Pseudo-Second Order Equation and the Sorbate Intraparticle Diffusivity. *Adsorption* **2013**, *19* (5), 1055–1064.

(32) Umpleby, R. J.; Baxter, S. C.; Chen, Y.; Shah, R. N.; Shimizu, K. D. Characterization of Molecularly Imprinted Polymers with the Langmuir–Freundlich Isotherm. *Anal. Chem.* **2001**, *73* (19), 4584–4591.

(33) Moussa, M.; Ndiaye, M. M.; Pinta, T.; Pichon, V.; Vercouter, T.; Delaunay, N. Selective Solid Phase Extraction of Lanthanides from Tap and River Waters with Ion Imprinted Polymers. *Anal. Chim. Acta* **2017**, *963*, 44–52.

(34) Zheng, X.; Zhang, F.; Liu, E.; Xu, X.; Yan, Y. Efficient Recovery of Neodymium in Acidic System by Free-Standing Dual-Template Docking Oriented Ionic Imprinted Mesoporous Films. *ACS Appl. Mater. Interfaces* **2017**, *9* (1), 730–739.

(35) Wilfong, W. C.; Kail, B. W.; Bank, T. L.; Howard, B. H.; Gray, M. L. Recovering Rare Earth Elements from Aqueous Solution with Porous Amine–Epoxy Networks. *ACS Appl. Mater. Interfaces* **2017**, *9* (21), 18283–18294.

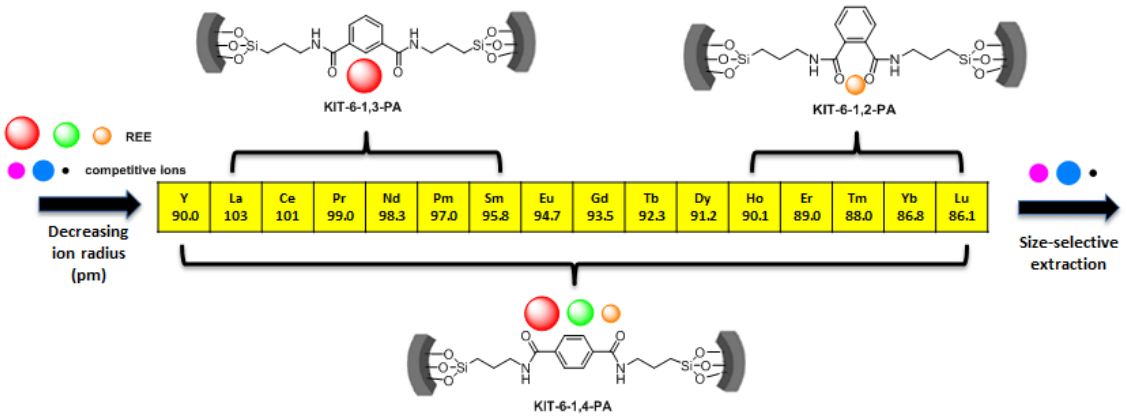
(36) Qi, X.-H.; Du, K.-Z.; Feng, M.-L.; Gao, Y.-J.; Huang, X.-Y.; Kanatzidis, M. G. Layered $A_2Sn_3S_7{\cdot}1.25H_2O$ (A = Organic Cation) as Efficient Ion-Exchanger for Rare Earth Element Recovery. *J. Am. Chem. Soc.* **2017**, *139* (12), 4314–4317.

(37) Li, C.; Zhuang, Z.; Huang, F.; Wu, Z.; Hong, Y.; Lin, Z. Recycling Rare Earth Elements from Industrial Wastewater with Flowerlike Nano-$Mg(OH)_2$. *ACS Appl. Mater. Interfaces* **2013**, *5* (19), 9719–9725.

(38) Zhang, H.; McDowell, R. G.; Martin, L. R.; Qiang, Y. Selective Extraction of Heavy and Light Lanthanides from Aqueous Solution by Advanced Magnetic Nanosorbents. *ACS Appl. Mater. Interfaces* **2016**, *8* (14), 9523–9531.

(39) Dupont, D.; Brullot, W.; Bloemen, M.; Verbiest, T.; Binnemans, K. Selective Uptake of Rare Earths from Aqueous Solutions by EDTA-Functionalized Magnetic and Nonmagnetic Nanoparticles. *ACS Appl. Mater. Interfaces* **2014**, *6* (7), 4980–4988.

(40) Lefrançois-Perreault, L.; Giret, S.; Gagnon, M.; Florek, J.; Larivière, D.; Kleitz, F. Functionalization of Mesoporous Carbon Materials for Selective Separation of Lanthanides under Acidic Conditions. *ACS Appl. Mater. Interfaces* **2017**, *9* (13), 12003–12012.


KIT-6-1,3-PA
KIT-6-1,2-PA
REE
competitive ions
Y 90.0
La 103
Ce 101
Pr 99.0
Nd 98.3
Pm 97.0
Sm 95.8
Eu 94.7
Gd 93.5
Tb 92.3
Dy 91.2
Ho 90.1
Er 89.0
Tm 88.0
Yb 86.8
Lu 86.1
Decreasing ion radius (pm)
Size-selective extraction
KIT-6-1,4-PA